Journal of Anatomy

J. Anat. (2015) **227**, pp341–351 doi: 10.1111/joa.12342

Feeding biomechanics of the cownose ray, *Rhinoptera bonasus*, over ontogeny

Matthew A. Kolmann,[1] Daniel R. Huber,[2] Philip J. Motta[3] and R. Dean Grubbs[4]

[1]*Department of Biological Science, Florida State University, Tallahassee, FL, USA*
[2]*Department of Biology, University of Tampa, Tampa, FL, USA*
[3]*Department of Integrative Biology, University of South Florida, Tampa, FL, USA*
[4]*Florida State University Coastal and Marine Laboratory, St Teresa, FL, USA*

Abstract

Growth affects the performance of structure, so the pattern of growth must influence the role of a structure and an organism. Because animal performance is linked to morphological specialization, ontogenetic change in size may influence an organism's biological role. High bite force generation is presumably selected for in durophagous taxa. Therefore, these animals provide an excellent study system for investigating biomechanical consequences of growth on performance. An ontogenetic series of 27 cownose rays (*Rhinoptera bonasus*) were dissected in order to develop a biomechanical model of the feeding mechanism, which was then compared with bite forces measured from live rays. Mechanical advantage of the feeding apparatus was generally conserved throughout ontogeny, while an increase in the mass and cross-sectional area of the jaw adductors resulted in allometric gains in bite force generation. Of primary importance to forceful biting in this taxon is the use of a fibrocartilaginous tendon associated with the insertion of the primary jaw adductor division. This tendon may serve to redirect muscle forces anteriorly, transmitting them within the plane of biting. Measured bite forces obtained through electrostimulation of the jaw adductors in live rays were higher than predicted, possibly due to differences in specific tension of actual batoid muscle and that used in the model. Mass-specific bite forces in these rays are the highest recorded for elasmobranchs. Cownose rays exemplify a species that, through allometric growth of bite performance and morphological novelties, have expanded their ecological performance over ontogeny.
Key words: batoid; biological pulley; bite force; durophagy; elasmobranch; performance.

Introduction

Growth affects the performance of structures, and therefore resource use, such that it ultimately impacts an organism's niche throughout its ontogeny (Erickson et al. 2003; Vincent et al. 2007). This ontogenetic form–function paradigm is complicated for predators by the fact that the structural and functional properties of their prey (e.g. skeletal strength or elusiveness) vary considerably among taxa. For durophagous animals, composite biological materials such as mollusk shell or crustacean calcified-chitin present significant challenges to prey capture and processing (Palmer, 1979; Korff & Wainwright, 2004). Bite force has been shown to be a relevant metric of feeding performance in durophagous taxa. This trait is critical to successful feeding events and presumably has been selected for in these taxa (Santana & Dumont, 2009; Pfaller et al. 2011).

Positive allometric gains in bite force across durophagous taxa have been shown to increase dietary breadth (Binder & van Valkenburgh, 2000; Verwaijen et al. 2002), permit earlier access to durable prey (ontogenetically), reduce competition and promote rapid growth in juvenile animals (Binder & van Valkenburgh, 2000; Kolmann & Huber, 2009). Furthermore, durophagous vertebrates exhibit convergent morphological traits, including molariform dentition, reinforced jaw and cranial skeletons, high-leverage and hypertrophied jaw adductor musculature (teleosts – Hernandez & Motta, 1997; sharks – Habegger et al. 2012; turtles – Herrel et al. 2002; finches – Van der Meij & Bout, 2004; bats – Santana et al. 2010). This tendency towards convergence is evident even in the scaling of general anatomical trends with respect to performance: while bite force generally scales positively with increasing body size, in durophagous taxa bite force scales closely with head width (HW), generally a function of large jaw adducting muscles (Anderson et al. 2008).

Correspondence
Matthew A. Kolmann, Department of Ecology and Evolutionary Biology, University of Toronto Scarborough, 1265 Military Trail, Toronto, ON, Canada M1C 1A4. T: +647 218 2253; E: matthew.kolmann@mail.utoronto.ca

Accepted for publication *27 May 2015*
Article published online *16 July 2015*

Durophagous cartilaginous fishes exhibit many of these characteristics despite having a more ductile skeleton than their bony counterparts (Summers, 2000). Cownose rays (Rhinopterinae) and other myliobatid stingrays are exemplars of convergent trait evolution with other vertebrate durophages in that they consume small bivalves, gastropods and crustaceans at all stages of their ontogeny (Gray et al. 1997; Yamaguchi et al. 2005; Ajemian & Powers, 2012), and possess characteristics such as: grinding tooth plates, trabecular-reinforced jaw skeletons, fused jaw symphyses and massive pennate-fibered jaw adductors with fibrocartilaginous pads that wrap around the corners of the jaw (Summers, 2000; Aschliman, 2014; Kolmann et al. 2014). These stingrays have a euhyostylic jaw suspension in which the jaws are disarticulated from the cranium and the paired hyomandibulae provide indirect attachment (Dean et al. 2007), such that mechanisms of strain dissipation and stress reduction during feeding may be altogether different than observed in other durophagous vertebrates (Huber et al. 2005). Nonetheless, the manner in which myliobatid rays generate presumably high bite forces has not been quantified, nor has the manner in which their feeding morphology and performance change over ontogeny.

The specific objectives of this study were to: (i) investigate which anatomical and physiological traits contribute to bite force generation in euhyostylic cownose rays; (ii) determine the scaling pattern of bite force over ontogeny; and (iii) examine the accuracy of the theoretical bite force modeling through comparison with *in vivo* bite force measurement in live stingrays. It is hypothesized that: (i) increases in size of the jaw adductor musculature will facilitate positive allometry of bite force, as is typical of other durophagous vertebrates; (ii) theoretical bite force will be an accurate predictor of *in vivo* tetanic bite force; and (iii) in terms of general morphometrics, bite force will scale with more conservative measurements of HW (interspiracular distance), owing to the laterally confining nature of the pectoral propterygia.

Materials and methods

Specimen collection

Rhinoptera bonasus ($n = 27$) were collected primarily via fisheries independent methods in collaboration with several agencies and institutes: National Marine Fisheries Service (NMFS) Panama City Lab; Florida Fish and Wildlife Commission (FWC) Charlotte Harbor and Eastpoint Labs; and during NMFS GulfSPAN surveys of elasmobranch diversity. All animals were killed by severing of the spinal column or by placing the animal on ice in accordance with Institutional Animal Care and Use Committee guidelines (protocol #: 1118 Grubbs) at Florida State University or by the guidelines of each respective agency. Disk width (DW), sex and maturity were recorded upon capture. Most stingrays were collected between Panama City in the northwestern panhandle region of Florida south to Charlotte Harbor. In addition, live specimens ($n = 6$) were collected with monofilament gillnets of 3.5 cm square mesh size (SAL-11-1092-SR).

Jaw adductor muscle anatomy

Prior to dissection, specimens were decapitated posterior to the branchial region, and cranial morphometrics taken with digital calipers to determine how bite force, muscle cross-sectional area (CSA) and lever mechanics scale with head dimensions. These morphometrics included prebranchial length (distance measured from the tip of the rostral lobes to the first gill opening), HW [transverse distance from the first gill opening to the corresponding gill slit on the opposite (left or right) side of the animal], head height (measured from the first gill opening to the most dorsal point of the cranial fontanelle), inter-spiracle distance (measured as the distance between the spiracles taken from the dorso-posterior-most point of the spiracle cavity) and inter-orbital distance (IO; measured as the minimum distance between the orbits). Specimens were skinned and the jaw adductor complex removed from the cranium by severing of the chondrocranial–hyomandibular ligament and associated musculature. The superficial fascia covering the jaw adductor musculature was removed to allow closer observation of muscular divisions and myofiber directionality. The nomenclature and relative insertion and origin points of these muscles follow Kolmann et al. (2014; Fig. 1), which draws from Miyake et al. (1992), Lovejoy (1996), and Dean & Motta (2004a).

Theoretical bite force modeling

For each specimen, all jaw adductor subdivisions were excised from the jaw skeletal structure. The origin and insertion of each muscle subdivision, the position of the jaw joint and the bite points were recorded relative to the origin of a three-dimensional coordinate system (antero-medial tip of the palatoquadrate), and the relative positions of these elements were determined by measuring their distances from the *X-*, *Y-* and *Z*-planes intersecting at the origin (Huber & Motta, 2004; Huber et al. 2005, 2006, 2008).

To determine relative muscle force, which is proportional to the anatomical CSA (cm^2), each parallel-fibered muscle (the suborbitalis and adductor mandibulae – lateralis, deep, lingualis and medialis) was sectioned through its center of mass perpendicular to the fiber angle. All muscle cross-sections were then photographed using a digital camera (EOS Rebel; Canon, Lake Success, New York, NY, USA) and the CSA determined using ImageJ (ImageJ version 1.40; National Institute of Health, Bethesda, MD, USA). Pennate-fibered muscles (adductor mandibulae major – AMMa) require the physiological CSA (PCSA; cm^2) to estimate relative muscle force (Gans & Gaunt, 1991). To determine PCSA, average fiber lengths (cm), average pennation angle (Ø – the angle at which fibers attach to the central tendon) and average muscle fiber density for fishes (1.05 g cm^{-3}; Wainwright, 1988) were incorporated into an equation by Powell et al. (1984):

$$\text{Physiological CSA} : P_{CSA} = \frac{\text{muscle mass}}{\text{muscle density}} \times \frac{\cos \emptyset}{\text{fiber length}} \quad (1)$$

Finally, relative muscle force or theoretical maximum tetanic tension (P_O; N) for each jaw adductor was determined by multiplying the CSA of the muscle by the specific tension (T_S; N) of shark red muscle as this is not determined for batoids (14.2 Nm^{-2}; Lou et al. 2002):

$$\text{Maximum tetanic tension} : P_O = \text{CSA} * T_S \quad (2)$$

Force vectors were then generated for each of the muscles using their maximum P_O, and positions of origin and insertion.

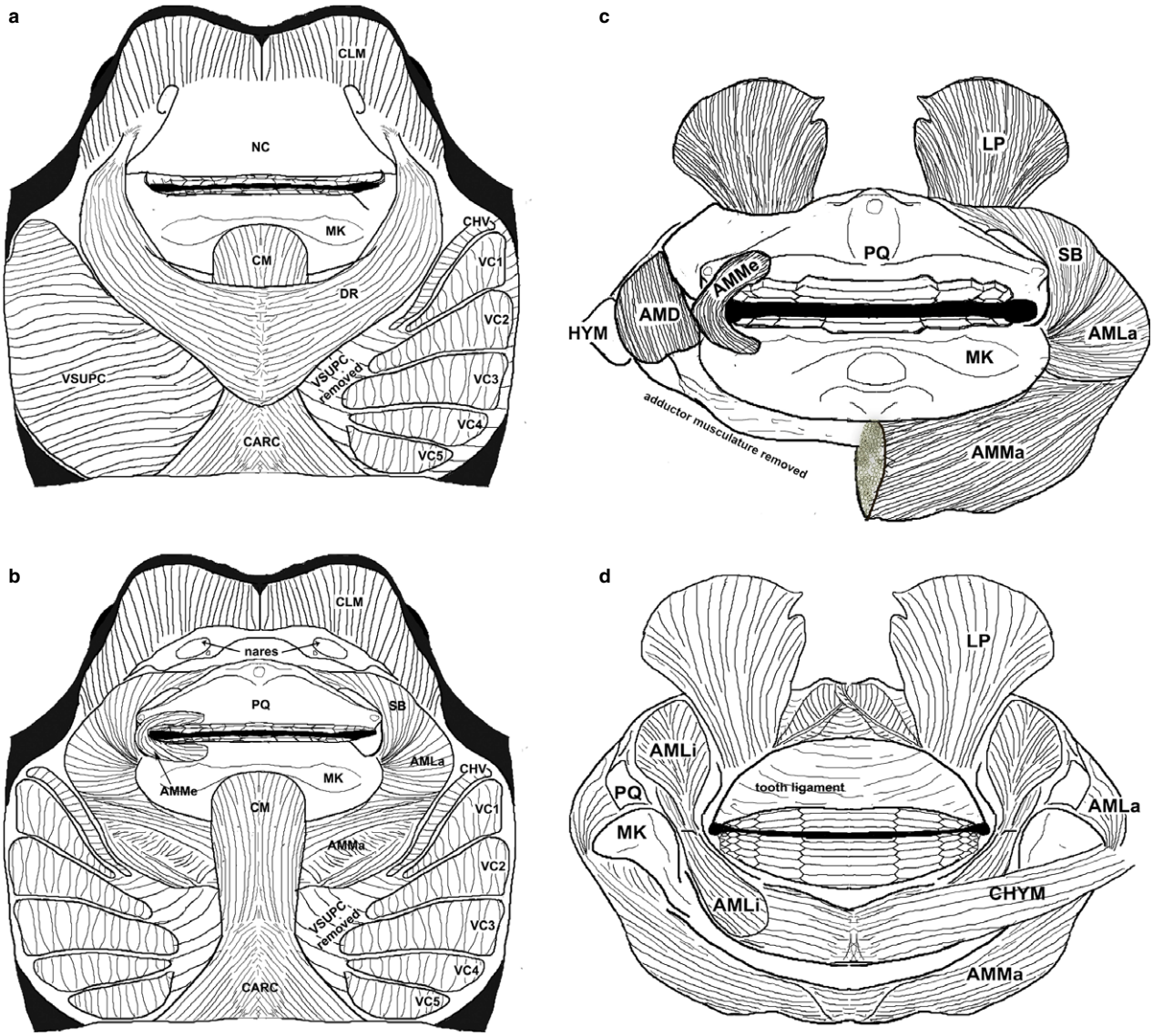

Fig. 1 Cranial musculature of *Rhinoptera bonasus*. (a) Superficial and (b) deep ventral views of musculature; (c) ventral and (d) dorsal aspects of the upper and lower jaws removed from the cranium. AMD, adductor mandibulae deep; AMLa, adductor mandibulae lateralis; AMLi, adductor mandibulae lingualis; AMMa, adductor mandibulae major; AMMe, adductor mandibulae medialis; CARC, coracoarcualis; CHV, constrictor hyoideus ventralis; CHYM, coracohyomandibularis; CLM, cephalic lobe muscles; CM, coracomandibularis; DR, depressor rostri; HYM, hyomandibular cartilage; LP, levator palatoquadrati; MK, Meckel's cartilage; NC, nasal curtain; PQ, palatoquadrate; SB, suborbitalis; VC1–5, ventral constrictors; VSUPC, constrictor superficiales ventrales.

In-lever (L_I) distances were calculated using the points of attachment of each muscle on the lower jaw and the jaw joint (Fig. 2). A resultant in-lever distance (RL_I) was determined by using a weighted average of all the muscle in-levers, with weighting based on the overall force contribution of each muscle to total muscular force (Huber et al. 2005). Out-lever (L_O) distances were based on the positions of the lateral and medial bite points (LBP and MBP) in comparison to the jaw joint (Fig. 2). Two bite points were determined for the lower jaw by examination of tooth occlusion and wear patterns; a MBP was located at the tooth plate in the medial tooth row where occlusion occurred and wear was greatest, and a LBP was located at the second-most lingual tooth row, directly across from the MBP (Fig. 2). Mechanical advantage (MA) at both the MBP and LBP was then calculated by dividing the resultant L_I by each respective L_O. The primary jaw adductor (AMMa) attaches to the palatoquadrate via a large, robust tendon. Within this tendon is a fibrocartilage pad that cushions the tendon from the lateral margins of the Meckel's cartilage (Summers et al., 2003) and may reroute force from the lateral plane (*Z*-direction) to the vertical plane (*Y*-direction). To address this, the MA and bite forces of the feeding mechanism of *R. bonasus* have been modeled with the insertion of the primary jaw adductor (AMMa) at the interface of the right and left antimeres of the muscle (Fig. 1c), as well as at the location of this fibrocartilage pad (Fig. 1c).

A static equilibrium model, which calculates a summation of the bending moments generated by the jaw adducting musculature

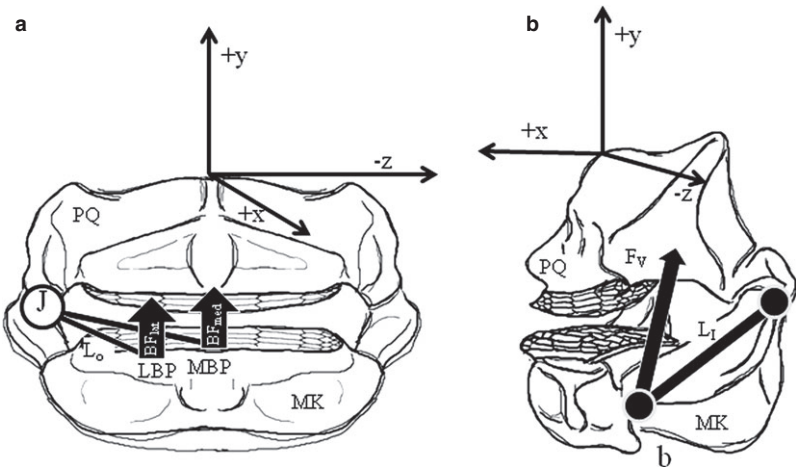

Fig. 2 Schematic of jaw lever systems in *Rhinoptera bonasus*. (a, b) Ventral and lateral aspects of the upper and lower jaws removed from the cranium with three-dimensional system diagram, (a) free-body diagram of out-lever distances, (b) resultant muscle in-lever distance. AMD, adductor mandibulae deep; AMLa, adductor mandibulae lateralis; AMLi, adductor mandibulae lingualis; AMMa, adductor mandibulae major; AMMe, adductor mandibulae medialis; BF_{med}/BF_{lat}, medial/lateral bite forces; FV, resolved adductor force vector; J, jaw joint; L_I, in-lever; L_O, out-lever; MK: Meckel's cartilage; PQ, palatoquadrate; SB, suborbitalis.

about the jaw joints, was used to predict theoretical maximum medial and lateral bite forces (BF_{med} and BF_{lat}, respectively; Huber et al. 2005). The static equilibrium of all the forces acting on the lower jaw (F_{LJ}) is represented by:

$$\Sigma F_{LJ} = F_{JR} + F_{AMMe} + F_{SB} + F_{AMLa} + F_{AMMa} + F_{AMD} + F_{AMLi} + F_B = 0, \quad (3)$$

where F_{JR} is the joint reaction force (which balances bite force and allows summation to 0), F_B is the bite force occurring for a given prey item at one of the bite points, while F_{AMMe}, F_{SB}, F_{AMLa}, F_{AMMa}, F_{AMD}, F_{AMLi} are the adductor muscle forces acting upon the lower jaw (Fig. 1c).

In vivo bite measurement

Six cownose rays, distributed across the average size range of the species (31–79.5 cm DW, mixed males and females in good condition post-capture) were anesthetized and perfused with a recirculating solution of buffered MS-222 (tricaine methanesulfonate: 0.1 g L^{-1}) during stimulation trials. The primary jaw adductor complex was implanted bilaterally with stainless steel 23-gage hypodermic needles (two sets of three needles per side of the head per ray per stimulation) connected to a physiological pulse stimulator (Model SD9; Grass Products, Warwick, RI, USA). In this manner, the AMMa, AM lateralis (AMLa) and suborbitalis (SB) were stimulated directly. The AM lingualis (AMLi) was not able to be stimulated due to its position on the dorsal face of the jaws. Tetanic fusion (tension or contraction) of these muscles was accomplished via stimulation (20–40 V, 60 Hz, 1.0 ms duration, biphasic AC current) while a piezoelectric load cell (Model 201B02; PCB Piezotronics, Depew, NY, USA), fitted with lever arms, was positioned at the MBP on the lower jaw. Bite force data measured from the force transducer were recorded via a 6020E data acquisition board and LabView v.6.0 software (National Instruments, Austin, TX, USA). Three recorded measurements were taken from each individual, per trial. Implanted muscles were allowed a recovery period of 2 min between each 3–5 s stimulation. Specimens underwent two series of trials, with a minimum of 3 h between stimulations. After stimulations, individuals were ventilated with aerated seawater (sans MS-222) until consciousness was regained, after which rays were placed back in holding tanks and observed during recovery. Afterwards, animals were killed using an overdose of MS-222 (1 g L^{-}) and bite forces were determined using the previously described biomechanical modeling procedures in order to examine the extent to which modeling predicted *in vivo* performance. Only single maximum measured bite forces recorded from each animal were used in the analysis.

Statistical analysis

Data were log-transformed after plotting all raw data (excluding MA and jaw adductor fiber angle), which showed non-normal distributions. Cranial morphometrics, muscle forces, masses and CSAs, lever distances, and fiber lengths of pennate-fibered muscles were log-transformed and regressed against log-transformed body size (straight disk width, DW) using reduced major axis (RMA) regression. MA values were not transformed and appear on a semi-log scale in the following figures (Pfaller et al. 2011). The nature of the scaling relationship between a variable and body size (DW) was determined by comparing the slope of the regression to the expected isometric slope predicted by Euclidean geometry (MA and fiber angles = 0; morphometrics and lever distances = 1; CSAs and forces = 2; muscle masses = 3). Confidence intervals were generated around regression slopes and compared with the expected isometric slope for each variable in order to determine allometry (positive or negative) or isometry (Pfaller et al. 2011). Isometry was indicated by regression slope confidence intervals straddling the isometric slope value, whereas regression slope confidence intervals above or below the isometric slope indicated positive or negative allometry, respectively (Pfaller et al. 2011). This type of analysis was also repeated in order to determine the scaling relationship between cranial morphometrics and bite force (medial and lateral). Medial (i.e. anterior) bite force data from other durophagous elasmobranchs were gathered from the literature (Huber et al. 2008), log-transformed and regressed against log-body mass. The residuals of this relationship represent mass-specific bite forces (Huber et al. 2008) and were used to compare feeding performance among durophagous chondrichthyans.

In order to determine the accuracy of the biomechanical model, ontogenetic trends in theoretical and *in vivo* measured bite force values were compared using analysis of covariance (ANCOVA) on medial bite forces. A test of the homogeneity of slopes was used to determine if slopes of these relationships were significantly different. 'Stimulated' or 'estimated' dummy variables were classified as

covariates in the analysis. Regressions (RMA) and ANCOVAS were performed in R (version 2.15.0, www.theRproject.org).

Results

The AMMa produced the greatest theoretical muscle force (54.7 ± 1.3%) of all of the adductor muscle divisions across all stingray sizes (Table 1). The remaining adductor muscle divisions in order of decreasing magnitude of force production were the SB (13.94 ± 0.46%), AMLa (12.8 ± 0.98%), AMLi (9.46 ± 0.9%), AM deep (AMD; 7.31 ± 0.35%) and AM medialis (AMMe; 1.75 ± 0.13%; Table 1; Fig. 2). Muscle masses of all jaw adductors scaled with positive allometry over ontogeny in *R. bonasus* (Supporting Information, Fig. 3). Muscle CSA scaled with positive allometry for three of the six jaw adductors (SB, AMLa and AMMa; Supporting Information), although only two (SB: slope = 2.59; and AMMa: slope = 2.67) of the jaw adductor forces scaled with positive allometry (Supporting Information). However, all muscle CSAs and forces that scaled isometrically were only narrowly bounded by the confidence intervals around their slopes, suggesting that several muscle CSAs (and following that, muscle forces) are approaching allometric growth. AMMa mean fiber length scaled isometrically with respect to DW (slope = 1.06; Supporting Information), while mean fiber angle scaled with positive allometry (slope = 0.41; Supporting Information).

For all lever models, the resultant in-lever (without fibrocartilage: slope = 0.97; with fibrocartilage: slope = 0.93), and the medial (slope = 1.01) and lateral (slope = 1.00) outlevers (Fig. 4; Supporting Information) scaled isometrically. Considering an aponeurotic insertion for the primary jaw adductor [i.e. AMMa originating at its antimere on the ventral surface of the jaw, rather than originating at the fibrocartilage pad (lateral sides of the jaws)], medial MA ranged from 0.80 to 0.98 (Fig. 5; Supporting Information), while lateral MA ranged from 1.07 to 1.48 over the ontogeny of *R. bonasus* (Fig. 4). Taking the fibrocartilage pad as the insertion of the AMMa decreases both medial (0.49–0.72; Fig. 5) and lateral (0.68–1.06; Fig. 5; Supporting Information) MA in this scenario.

Considering a jaw lever system with an antimeric insertion of the AMMa, medial (25–336 N; Fig. 6) and lateral (25–362 N; Fig. 6) bite forces scaled with positive allometry (medial bite force: slope = 2.39; lateral bite force: slope = 2.36; Table 2). Alternatively, using the fibrocartilage pad as the origin of the AMMa results in higher medial (25–480 N; Fig. 6) and lateral (24–520 N; Fig. 6) bite forces, both of which scaled with positive allometry over ontogeny (medial bite force: slope = 2.59; lateral bite force: slope = 2.62; Fig. 6; Table 2). Augmentation of bite force in this arrangement is presumably because of the redirection of muscle force orthogonal to the biting surface of the jaw. Overall, positive allometry of bite force in both models is attributable to positive allometry of multiple jaw adductor forces particularly that of the primary jaw adductor, the AMMa (Supporting Information).

Bite forces measured during tetanic stimulation increased with positive allometry over ontogeny and had comparatively similar slope to theoretical medial bite force with use of the fibrocartilage (slope = 2.55 vs. 2.59, respectively; Table 3). ANCOVA indicated that the interaction of the covariates (stimulated vs. estimated) was not significantly different, i.e. the difference in the mean slope of the estimated medial bite forces did not differ significantly from the measured bite forces ($F = 0.094$, $P = 0.761$, residual standard error = 0.0698). However, the intercept of this regression (*Y*-int. = −4.92) was marginally higher than the estimated regression of bite force vs. DW, suggesting that despite capturing the relationship between bite performance and mass, the biomechanical estimates of bite force underestimated overall bite force.

Table 1 Descriptive statistics for musculoskeletal variables and bite force generation in *Rhinoptera bonasus*.

Muscle division	Mass (g)	CSA (cm^2)	In-lever (cm)	Muscle force (N)	Percent contribution to bite force (N)
AMMe	0.66 ± 0.09	0.17 ± 0.03	3.04 ± 0.17	2.23 ± 0.23	1.75 ± 0.13
	0.01–1.69	0.03–0.69	1.52–4.63	0.47–4.92	0.85–3.85
SB	4.32 ± 0.64	1.39 ± 0.17	2.79 ± 0.17	20.7 ± 2.55	13.94 ± 0.46
	0.10–12.13	0.18–3.351	1.55–4.6	2.61–49.93	9.6–18.49
AMLa	2.81 ± 0.42	1.19 ± 0.14	2.79 ± 0.17	17.84 ± 2.13	12.79 ± 0.98
	0.1–6.68	0.22–2.73	1.55–4.6	3.35–40.74	6.81–36.22
AMD	1.57 ± 0.24	0.69 ± 0.08	1.69 ± 0.12	10.2 ± 1.12	7.31 ± 0.35
	0.08–4.75	0.14–1.45	0.64–3.62	2.2–21.6	4.71–10.71
AMMa	14.84 ± 2.18	5.48 ± 0.65	2.28 ± 0.13	81.6 ± 9.67	54.74 ± 1.34
	0.6–39.3	0.52–14.72	1.18–3.37	7.75–219.33	30.51–62.36
AMLi	3.43 ± 0.48	0.84 ± 0.08	2.96 ± 0.17	12.51 ± 1.26	9.46 ± 0.9
	0.08–7.93	0.14–1.62	1.7–4.82	2.02–24.1	5.78–31.31

Values are the mean ± SEM.AMD, adductor mandibulae deep; AMLa, adductor mandibulae lateralis; AMLi, adductor mandibulae linguales; AMMa, adductor mandibulae major; AMMe, adductor mandibulae medialis; CSA, cross-sectional area; SB, suborbitalis.

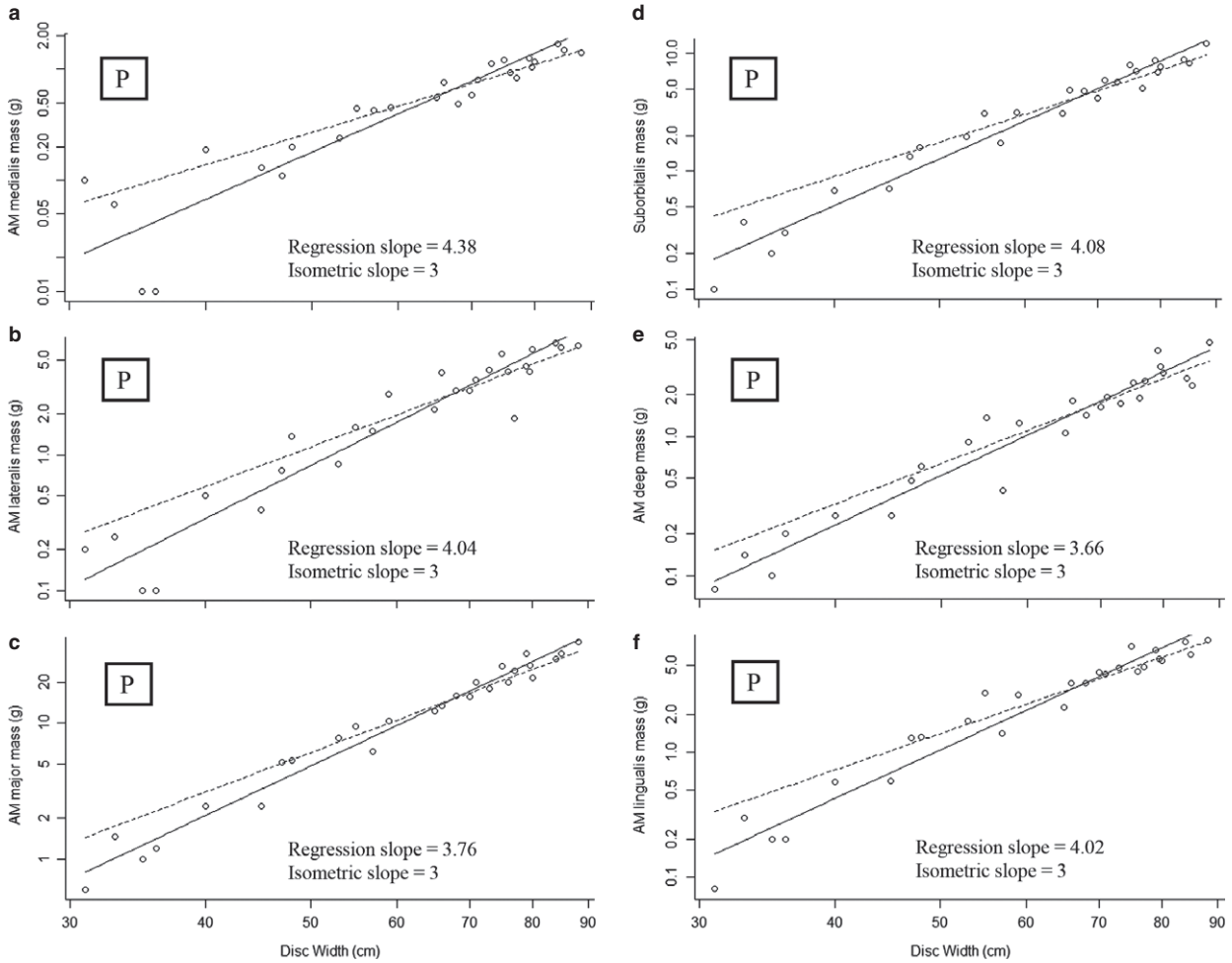

Fig. 3 Jaw adductor muscle mass (g) over ontogeny in *Rhinoptera bonasus*. Solid lines, RMA regressions for the data; dashed lines, scaling predictions based on isometric growth set to cross data lines at the mean values of each independent variable. (a) SB muscle masses, (b) AMD muscle masses, (c) AMMa muscle masses, (d) AMMe muscle masses, (e) AMLi muscle masses, (f) AMLa muscle masses. 'I' denotes isometry, 'P' denotes positive allometry.

Cranial morphometrics all scaled isometrically with DW throughout the ontogenetic series (Supporting Information). Both medial and lateral bite forces (using the AMMa fibrocartilage pad as the insertion) scaled with positive allometry with respect to cranial morphometrics across all variables. IO showed the most predictive power with respect to both medial and lateral bite forces ($r^2 = 0.93$ and 0.92, respectively). Cownose rays generated the largest mass-specific bites of the cartilaginous fishes that have been investigated, followed by other durophagous taxa including the ratfishes *Hydrolagus colliei* and *Chimaera monstrosa*, and the horn shark *Heterodontus francisci* (Table 4).

Discussion

As hypothesized, positive allometry of feeding performance in cownose rays is driven by allometric growth of the jaw adductor muscles, particularly the massive AMMa. The AMMa produces over 54% of the muscular force in these durophagous rays (Table 1), despite an increase in average fiber length in this muscle, which should decrease force production per unit volume (Gans & Gaunt, 1991). The morphology of this muscle division is markedly different between durophagous rays and non-durophagous rays, with the AMMa in the former wrapping around the lower jaw like a sling (Kolmann et al. 2014). This arrangement maximizes use of cranial space in a system that is constrained laterally by the pectoral propterygia.

The rerouting of the adductor mandibulae force by its tendon and associated fibrocartilage pad from a more lateral direction, to aligned directly against the occlusal surface, results in a 70% increase in overall bite force generation compared with a hypothetical situation in which the fibrocartilage does not redirect force (Table 3). The lateral processes of the Meckel's cartilage form the 'blocks' of this Type-1 biological pulley system, where force is increased only by redirection, not by increasing MA (Benjamin et al. 1995; Benjamin & Ralphs, 1998). This arrange-

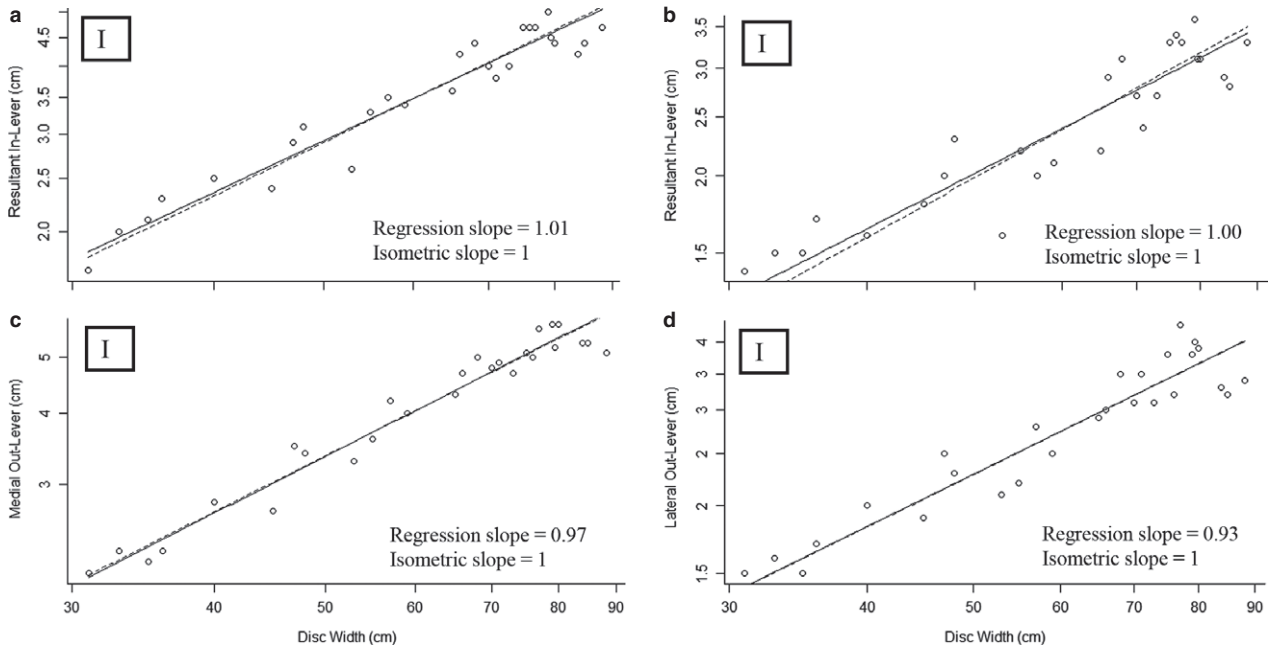

Fig. 4 Jaw lever distances (cm) over ontogeny in *Rhinoptera bonasus*. Solid lines, RMA regressions for the data; dashed lines, scaling predictions based on isometric growth set to cross data lines at the mean values of each independent variable. (a) Resultant in-lever distance, (b) resultant in-lever distance using the tendinous PQ insertion, (c) medial out-lever distance, (d) lateral out-lever distance. 'I' denotes isometry, 'P' denotes positive allometry.

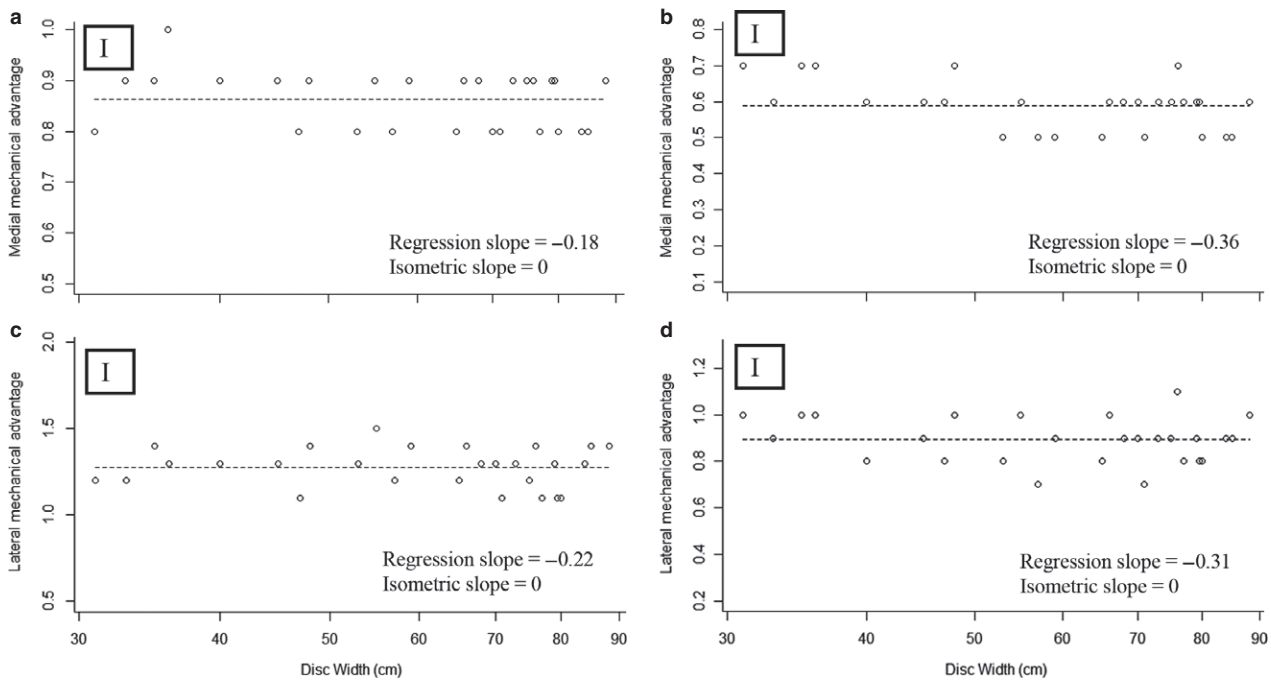

Fig. 5 MA of the jaw lever system over ontogeny in *Rhinoptera bonasus*. Solid lines, RMA regressions for the data; dashed lines, scaling predictions based on isometric growth set to cross data lines at the mean values of each independent variable. (a) Medial MA, (b) medial MA using the tendinous PQ insertion, (c) lateral MA, (d) lateral MA using the tendinous PQ insertion. 'I' denotes isometry, 'N' denotes negative allometry, 'P' denotes positive allometry.

ment of a jaw adductor muscle sling together with a Type-1 pulley system serves to maximize muscle force generation in a constrained cranial volume.

The MA of the jaw lever apparatus scales isometrically with respect to body size. Unlike most other elasmobranchs, which feature aponeurotic muscle insertions, cownose rays

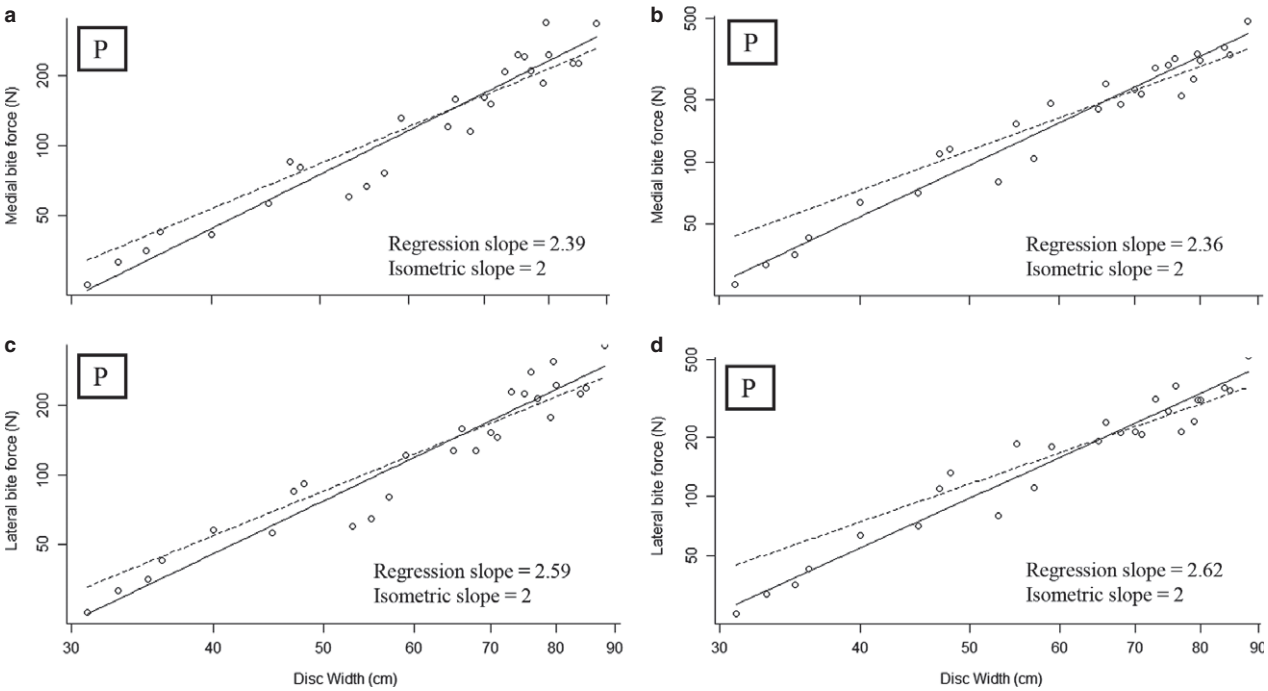

Fig. 6 Maximum theoretical bite forces (N) over ontogeny in *Rhinoptera bonasus*. Solid lines, RMA regressions for the data; dashed lines, scaling predictions based on isometric growth set to cross data lines at the mean values of each independent variable. (a) Medial bite force, (b) medial bite force using the tendinous PQ insertion, (c) lateral bite force, (d) lateral bite force using the tendinous PQ insertion, medial biting. 'I' denotes isometry, 'P' denotes positive allometry.

Table 2 Scaling of bite force scenarios in *Rhinoptera bonasus.*

Independent variables	r^2	Isometric slope	Intercept (*a*)	Slope (*b*)	CI	*P*	Scaling scenario
BF_{med} – measured	0.97	2	−4.92	2.55	2.072–3.138	9.68E-05	P
BF_{med}	0.93	2	−5.05	2.39	2.151–2.666	2.19E-16	P
BF_{lat}	0.93	2	−4.90	2.36	2.113–2.645	6.69E-16	P
BF_{med} – with fibrocartilage	0.95	2	−5.57	2.59	2.374–2.830	1.43E-18	P
BF_{lat} – with fibrocartilage	0.94	2	−5.65	2.62	2.369–2.888	2.92E-17	P

CI; confidence interval.
Independent variables scaled against DW. Significance level ($\alpha = 0.05$). Medial bite force (N): BF_{med}; lateral bite force (N): BF_{lat}, measured denotes *in vivo* data. For scaling scenarios: I = isometry; N = negative allometry; P = positive allometry.

Table 3 Descriptive statistics for bite force scenarios in *Rhinoptera bonasus.*

Muscle division	Medial (N)	Lateral (N)
Class 3 without fibrocartilage	144.0 ± 0.09 25.3–336.1	146.9 ± 0.03 25.3–362.1
Class 3 with fibrocartilage	194.8 ± 0.64 25.3–480.2	199.8 ± 0.65 25.3–520.2
Measured bite force	201.7 ± 0.24 50.8–561.1	

Values are the mean ± SEM. Range from smallest individual to largest.

have several jaw muscles with tendinous insertions (Summers, 2000; Summers et al. 2003). Direct tendinous insertions create regions of higher stress, which are disadvantageous for most elasmobranchs given the weakly-calcified nature of their jaws. However, the reinforced skeletal structure of durophagous rays may alleviate these internal stresses, thereby increasing the pull-out strength of muscles inserting via tendons (Summers, 2000; Summers et al. 2003), and aiding in force transfer from the jaw muscles to the skeleton during feeding. Nonetheless, direct tendon attachment in cownose rays may constrain their ability to shift muscle insertions over ontogeny without significant skeletal remodeling (which is impossible or improbable with

Table 4 Mass-specific analysis of bite forces across durophagous chondrichthyans.

Species	Common name	Mass (g)	ABF (N)	Residuals
*Sphyrna tiburo**	Bonnethead shark	2920.0	25.6	−1.422
Galeus melastomus†	Blackmouth catshark	742.1	11.8	−1.341
Squalus acanthias†	Spiny dogfish	386.0	8.1	−1.309
Carcharhinus limbatus‡	Blacktip shark	5618.0	104.0	−0.429
Sphyrna mokarran†	Great hammerhead shark	580598.0	2432.0	−0.174
Carcharhodon carcharias§	Great white shark	240000.0	1602.0	−0.039
*Etmopterus spinax**	Velvet belly lanternshark	190.8	21.1	0.088
Chiloscyllium plagiosum¶	White-spotted bamboo shark	1041.0	69.0	0.213
Carcharhinus leucas†	Bull shark	192976.1	2128.0	0.381
Heterodontus francisci¶	Horn shark	2604.0	148.0	0.404
Hydrolagus colliei¶	Spotted ratfish	452.0	69.0	0.734
Heptranchias perlo¶	Sevengill shark	1115.0	132.0	0.819
Chimaera monstrosa†	Giant chimaera	98.9	30.4	0.864
Rhinoptera bonasus	Cownose ray	6040.0	561.1	1.211

*Mara et al. (2009).
†Habegger et al. (2012).
‡Huber et al. (2006).
§Wroe et al. (2008).
¶Huber et al. (2008).

a cartilaginous skeleton; Dean et al. 2009), thereby limiting ontogenetic change in MA as has been observed in spotted ratfish (*H. colliei*), horn sharks (*H. francisci*; Kolmann & Huber, 2009), blacktip sharks (*C. limbatus*; Huber et al., 2006), and juvenile bull sharks (*C. leucas*; Habeggar et al., 2012).

The hypothesis that theoretical bite force will be an accurate predictor of *in vivo* tetanic bite force proved accurate reflecting the rate at which bite force increases with size, but not in magnitude. Values for muscle P_O are completely lacking for batoids, and the value used in this study was from a cold-temperate catshark *Scyliorhinus canicula* at 12 °C (Lou et al. 2002). Cownose rays have relatively high whole-body metabolic Q_{10} values for oxygen consumption and are sustained, pelagic swimmers, and it is expected that their muscle physiology be considerably different from cold-temperate elasmobranchs like scyliorhinids (Neer et al. 2006; Bernal et al. 2012). Cownose rays are a subtropical species, and the stimulation trials were conducted at approximately 28 °C. Greater than two-fold difference in temperature can increase contractile forces potentially two-fold, assuming a Q_{10} value of 1.3 for skeletal muscle (Bennet, 1984). Lou et al. (2002) used somitic trunk muscle from sharks, while in some vertebrates masticatory muscle performance has been shown to produce fiber strains 65% greater than trunk muscle (Hoh, 2002; Van Wassenbergh et al. 2007; Yamaguchi, 2007). Although a considerable literature exists comparing measured to estimated muscle performance during feeding, very few studies have explicitly addressed the Q_{10} effect of temperature on skeletal muscle during whole feeding apparatus modeling (but see Anderson & Deban, 2012).

Cownose rays are capable of generating the highest mass-specific bite forces of any elasmobranch studied to date. These forces are greater even than other durophagous elasmobranchs, including *Hydrolagus colliei* and the horn shark, *Heterodontus francisci* (Table 4). Cownose rays share a sling-like primary jaw adductor with durophagous ratfishes and hypertrophied musculature with horn sharks, common convergent mechanical designs for durophagy in elasmobranchs (Huber et al. 2005, 2008). The durophagous bonnethead shark, *Sphyrna tiburo*, has comparatively lower feeding performance, presumably dissembling shelled prey using behavioral and chemical methods over mechanical processing (Wilga & Motta, 2000; Mara et al. 2009), highlighting the diverse nature of strategies for durophagy in elasmobranchs overall. Unlike other durophagous taxa, bite force in cownose rays does not scale directly with HW, which in this study included the region bounded by the pectoral propterygia, but with a more constrained volume – the space between the spiracles. Superficially similar morphometrics (HW vs. spiracular width) in this case may then be nonpareil, suggesting that cranial constraints on volume can be influencing the performance of these animals during development.

As cownose rays increase in size from neonates through to adults (in this study, 31–88 cm DW), bite force generation increases approximately 15-fold. Cownose rays nearly double in size (from approximately 35 to 60 cm DW) within their first 6 months of age (Neer & Thompson, 2005; Fisher et al. 2013), equating to a seven-fold increase in bite force production, from neonates to young-of-the-year rays. This suggests that nearly half of the total gains in feeding performance across ontogeny are achieved within the first year of growth. Hypertrophy of jaw adductor musculature translates to positive allometry of feeding performance over ontogeny, which is a hallmark of vertebrate development (Herrel & Gibb, 2006), especially in durophagous taxa.

Conclusions

Cownose rays achieve allometric gains in bite force primarily through hypertrophy of the jaw adductor musculature,

particularly the AMMa. Muscular force is also efficiently harnessed in these rays through use of a fibrocartilage pad and tendon that redirect force from the AMMa into the occlusal plane, akin to a Type-1 biological pulley in theoretical systems. Muscular hypertrophy drives positive allometric gains in bite force across the ontogeny of these durophagous rays, allowing cownose rays to drastically increase their feeding performance within the first year of growth. These trends are consistent with what has been shown in other juvenile vertebrates, and durophagous animals in particular – that positive allometry of performance is a shared characteristic of early vertebrate development, particularly in dietary specialists.

Acknowledgements

The authors dedicate this manuscript to the memory of E. Chipouras, a mentor and teacher unsurpassed in the realms of ichthyology, vertebrate evolution and storytelling. The authors thank C. Bedore, D. Bethea, J. Christofferson, L. Hollensead, G. Poulakis, R. Fisher, Z. Boudreau, L. Harris, M. Jones, C. Kwapich, J. Pfeiffenberger, C. Peterson, T. Richards and M. Taylor for assistance with specimen collection. M. Daniels, B. Henderson, C. Koenig, D. Overlin and D. Tinsley built and maintained aquatic enclosures as well as facilitated animal transport. M. Dobrovetsky and D. Kay assisted with data collection and dissection. M. Dean has been indispensable with regards to advice on cranial anatomy, terminology and draft revisions. J. Soda, D. Slice, M.L. Habegger and L. Whitenack provided essential advice on statistical methods. P. Gignac and G. Erickson provided advice on experimental design, initial drafts and biomechanical modeling. A. Ferguson assisted with experimental procedure and data-recording. Special thanks go to the Florida State Coastal and Marine Laboratory (FSUCML) for providing an excellent facility for research and learning. Funding for this project was provided by a Florida State University Coastal and Marine Laboratory Graduate Research Grant to M.A.K., FSUCML start-up funding to R.D.G. and a University of Tampa Research Grant to D.R.H. Bite force equipment provided in part by the Porter Family Foundation to P.J.M.

Funding

Florida State University Coastal and Marine Laboratory graduate research grant to M.A.K., FSUCML start-up funding to R.D.G., and a University of Tampa research grant to D.R.H.

References

Ajemian MJ, Powers SP (2012) Habitat-specific feeding by cownose rays (*Rhinoptera bonasus*) of the northern Gulf of Mexico. *Environ Biol Fishes* **95**, 79–97.

Anderson CV, Deban SM (2012) Thermal effects on motor control and *in vitro* muscle dynamics of the ballistic tongue apparatus in chameleons. *J Exp Biol* **215**, 4345–4357.

Anderson RA, McBrayer LD, Herrel A (2008) Bite force in vertebrates: opportunities and caveats for use of a nonpareil whole-animal performance measure. *Biol J Linn Soc* **93**, 709–720.

Aschliman NC (2014) Interrelationships of the durophagous stingrays (Batoidea: Myliobatidae). *Environ Biol Fish* **97**, 967–979.

Benjamin M, Ralphs JR (1998) Fibrocartilage in tendons and ligaments – an adaptation to compressive load. *J Anat* **193**, 481–494.

Benjamin M, Qin S, Ralphs JR (1995) Fibrocartilage associated with human tendons and their pulleys. *J Anat* **187**, 625–633.

Bennet AF (1984) Thermal dependence of muscle function. *Am J Physiol* **247**, 217–229.

Bernal D, Carlson JK, Goldman KJ, et al. (2012) Energetics, metabolism, and endothermy in sharks and rays. In: *The Biology of Sharks and Their Relatives*, 2nd edn. (eds Carrier JC, Musick JA, Heithaus MR), pp. 211–237. Boca Raton, FL: CRC Press LLC.

Binder WJ, van Valkenburgh BV (2000) Development of bite strength and feeding behavior in juvenile spotted hyenas (*Crocuta crocuta*). *J Zool* **252**, 273–283.

Dean MN, Motta PJ (2004a) Anatomy and functional morphology of the feeding apparatus of the lesser electric ray, *Narcine brasiliensis* (Elasmobranchii: Batoidea). *J Morphol* **262**, 462–483.

Dean MN, Bizzarro JJ, Summers AP (2007) The evolution of cranial design, diet, and feeding mechanisms in batoid fishes. *Integr Comp Biol* **47**, 70–81.

Dean MN, Mull CG, Gorb SN, et al. (2009) Ontogeny of the tessellated skeleton: insight from the skeletal growth of the round stingray *Urobatis halleri*. *J Anat* **3**, 227–239.

Erickson GM, Lappin AK, Vliet KA (2003) The ontogeny of bite-force performance in American alligator (*Alligator mississippiensis*). *J Zool* **260**, 317–327.

Fisher RA, Call GC, Grubbs RD (2013) Age, growth, and reproductive biology of cownose rays in Chesapeake Bay. *Mar Coast Fish* **5**, 224–235.

Gans C, Gaunt AS (1991) Muscle architecture in relation to function. *J Biomech* **24**, 53–65.

Gray AE, Mulligan TJ, Hannah RW (1997) Food habits, occurrence and population structure of the bat ray, *Myliobatis californica*, in Humboldt Bay, California. *Environ Biol Fishes* **49**, 227–238.

Habegger ML, Motta PJ, Huber DR, et al. (2012) Feeding biomechanics and theoretical calculations of bite force in bull sharks (*Carcharhinus leucas*) during ontogeny. *Zoology* **115**, 354–364.

Hernandez LP, Motta PJ (1997) Trophic consequences of differential performance: ontogeny of oral jaw-crushing performance in the sheepshead, *Archosargus probatocephalus* (Teleostei, Sparidae). *J Zool* **243**, 737–756.

Herrel A, Gibb AC (2006) Ontogeny of performance in vertebrates. *Physiol Biochem Zool* **79**, 1–6.

Herrel A, O'Reilly JC, Richmond AM (2002) Evolution of bite performance in turtles. *J Evol Biol* **15**, 1083–1094.

Hoh JFY (2002) 'Superfast' or masticatory myosin and the evolution of jaw-closing muscles of vertebrates. *J Exp Biol* **205**, 2203–2210.

Huber DR, Motta PJ (2004) Comparative analysis of methods for determining bite force in the spiny dogfish *Squalus acanthias*. *J Exp Zool* **301**, 26–37.

Huber DR, Eason TG, Hueter RE, et al. (2005) Analysis of the bite force and mechanical design of the feeding mechanism of the durophagous horn shark *Heterodontus francisci*. *J Exp Biol* **208**, 3553–3571.

Huber DR, Weggelaar CL, Motta PJ (2006) Scaling of bite force in the blacktip shark *Carcharhinus limbatus*. *Zoology* **109**, 109–119.

Huber DR, Dean MN, Summers AP (2008) Hard prey, soft jaws and the ontogeny of feeding mechanics in the spotted ratfish, *Hydrolagus colliei*. *J R Soc Interface* **5**, 941–952.

Kolmann MA, Huber DR (2009) Scaling of feeding biomechanics in the horn shark *Heterodontus francisci*: ontogenetic constraints on durophagy. *Zoology* **112**, 351–361.

Kolmann MA, Huber DR, Dean MD, et al. (2014) Myological variability in a decoupled skeletal system: batoid cranial anatomy. *J Morphol* **275**, 862–881.

Korff WL, Wainwright PC (2004) Motor pattern control for increasing crushing force in the striped burrfish (*Chilomycterus schoepfi*). *Zoology* **107**, 335–346.

Lou F, Curtin NA, Woledge RC (2002) Isometric and isovelocity contractile performance of red muscle fibers from the dogfish *Scyliorhinus canicula*. *J Exp Biol* **205**, 1585–1595.

Lovejoy NR (1996) Systematics of myliobatid elasmobranchs: with emphasis on the phylogeny and historical biogeography of Neotropical freshwater stingrays (Potamotrygonidae: Rajiformes). *Zool J Linn Soc* **117**, 207–257.

Mara KR, Motta PJ, Huber DR (2009) Bite force and performance in the durophagous bonnethead shark, *Sphyrna tiburo*. *J Exp Zool* **311**, 1–11.

Miyake T, McEachern JD, Hall BK (1992) Edgeworth's legacy of cranial muscle development with an analysis of muscles in the ventral gill arch region of batoid fishes (Chondrichthyes: Batoidea). *J Morphol* **212**, 213–256.

Neer JA, Thompson BA (2005) Life history of the cownose ray, *Rhinoptera bonasus*, in the northern Gulf of Mexico, with comments on geographic variability in life history traits. *Environ Biol Fishes* **73**, 321–331.

Neer JA, Carlson JK, Thompson BA (2006) Standard oxygen consumption of seasonally acclimatized cownose rays, *Rhinoptera bonasus* (Mitchill 1815), in the northern Gulf of Mexico. *Fish Physiol Biochem* **32**, 67–71.

Palmer RA (1979) Fish predation and the evolution of gastropod shell sculpture: experimental and geographic evidence. *Evolution* **33**, 697–713.

Pfaller JB, Gignac PM, Erickson GM (2011) Ontogenetic changes in jaw-muscle architecture facilitate durophagy in the turtle *Sternotherus minor*. *J Exp Biol* **214**, 1655–1667.

Powell PL, Roy RR, Kanim P, et al. (1984) Predictability of skeletal muscle tension from architectural determinations in guinea pigs. *J Appl Physiol* **57**, 1715–1721.

Santana SE, Dumont ER (2009) Connecting behavior and performance: the evolution of biting behavior and bite performance in bats. *J Evol Biol* **22**, 2131–2145.

Santana SE, Dumont ER, Davis JL (2010) Mechanics of bite force production and its relationship to diet in bats. *Funct Ecol* **24**, 776–784.

Summers AP (2000) Stiffening the stingray skeleton – an investigation of durophagy in myliobatid stingrays (Chondrichthyes, Batoidea, Myliobatidae). *J Morphol* **243**, 113–126.

Summers AP, Koob-Emunds MM, Kaijura SM, et al. (2003) A novel fibrocartilaginous tendon from an elasmobranch fish (*Rhinoptera bonasus*). *Cell Tissue Res* **312**, 221–227.

Van der Meij MAA, Bout RG (2004) Scaling of jaw muscle size and maximal bite force in finches. *J Exp Biol* **207**, 2745–2753.

Van Wassenbergh S, Herrel A, James RS, et al. (2007) Scaling of contractile properties of catfish feeding muscles. *J Exp Biol* **210**, 1183–1193.

Verwaijen D, van Damme R, Herrel A (2002) Relationships between head size, bite force, prey handling efficiency and diet in two sympatric lacertid lizards. *Funct Ecol* **16**, 842–850.

Vincent SE, Moon BR, Herrel A, et al. (2007) Are ontogenetic shifts in diet linked to shifts in feeding mechanics? Scaling of the feeding apparatus in banded watersnake *Nerodia fasciata*. *J Exp Biol* **210**, 205–2069.

Wainwright PC (1988) Morphology and ecology: functional basis of feeding constraints in Caribbean labrid fishes. *Ecology* **69**, 635–645.

Wilga CD, Motta PJ (2000) Durophagy in sharks: feeding mechanics of the hammerhead *Sphyrna tiburo*. *J Exp Biol* **203**, 2781–2796.

Wroe S, Huber DR, Lowry M, McHenry C, Moreno K, Clausen P, Ferrera TL, Cunningham E, Dean MN, Summers AP (2008) Three-dimensional computer analysis of white shark jaw mechanics: how hard can a great white bite? *J Zool.* **276**, 336–342.

Yamaguchi M (2007) Structure and function of masticatory (superfast) myosin. *J Oral Biosci* **49**, 216–218.

Yamaguchi A, Kawahara I, Ito S (2005) Occurrence, growth and food of longheaded eagle ray, *Aetobatus flagellum*, in Ariake Sound, Kyushu, Japan. *Environ Biol Fishes* **74**, 229–238.

Supporting Information

Additional Supporting Information may be found in the online version of this article:

Table S1. Scaling of muscle masses, CSAs and forces in *Rhinoptera bonasus.*

Table S2. Scaling of levers and MA in *Rhinoptera bonasus.*

Table S3. Scaling of bite force with cranial morphometrics in *Rhinoptera bonasus.*

Fig. S1. Jaw adductor muscle CSAs (cm^2) over ontogeny in *Rhinoptera bonasus*.

Fig. S2. Jaw adductor muscle forces (N) over ontogeny in *Rhinoptera bonasus*.